Modeling and Simulation of Interface Dynamics in Fluids/Solids and Applications,
National University of Singapore (14 - 18 May 2018)

Equilibria for thin grain systems: Surface diffusion and grain migration

Amy Novick-Cohen[1]

[1]Department of Mathematics,
Technion–Israel Institute of Technology,
Haifa, Israel 320003

Thin Polycrystalline Materials:
Grains, Grain Boundaries, and Grain Boundary Migration

- **Polycrystalline materials:** solids composed of many **grains** or crystals, which vary in their size and crystalline lattice orientation.
- **Grain boundaries: interfaces** where different grains meet.
- **Thin** or **nano-thin layers:** material layers ranging in thickness from a fraction of a **nanometer** to several **microns**.
- Typically, grain boundaries **migrate** to **reduce surface free energy**.

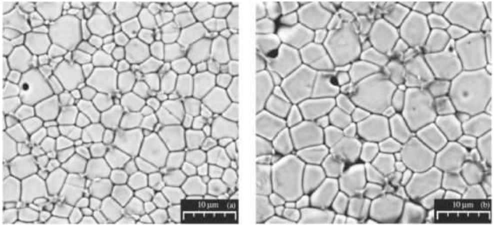

Figure 1: Sketch of grains and grain boundaries.

Classical features of interest

Grain boundary migration phenomena which effect thin film stability.

- Thermal grooving.
- Pitting at quadruple junctions.
- Wetting/dewetting and hole formation.

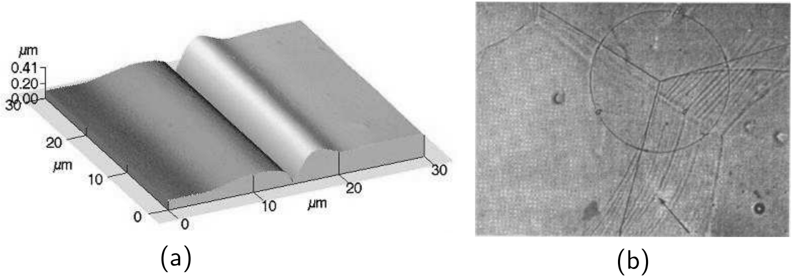

Figure 2: (a) Grooving. (b) Jerky motion.

Mullins' surface diffusion model

In 1957 Mullins proposed the 1-D nonlinear surface diffusion model:

$$y_t = -B[\kappa_x(1+y_x^2)^{-1/2}]_x, \quad \kappa = y_{xx}(1+y_x^2)^{-3/2}. \tag{1}$$

He linearized (1), obtaining the *Mullins' linear surface diffusion model:*

$$y_t = -By_{xxxx}, \tag{2}$$

by relying on a small slope assumption which is often physically relevant, then found solutions to (2) satisfying the initial and boundary conditions:

$$\begin{aligned} &y(x,0) = 0, \quad x \in [0,\infty), \\ &y_x(0,t) = m/2,\ y_{xx}(0,t) = 0,\ \lim_{x\to\infty} y(x,t) = 0, \quad t \in (0,\infty), \end{aligned} \tag{3}$$

in accordance with a simple symmetric thermal grooving model.

Mullins' solutions are classical, well studied, and used in estimating B.
Question: Do there exist other physically meaningful solutions to (2)?

Solutions to the Mullins' linear surface diffusion model

At to physical solutions, it seems reasonable to require

$$\lim_{x\to\infty} y(x,t) = 0. \tag{4}$$

Together with H. Kalantarova (2018), we found a 2 parameter family of solutions to (2),(4), of the self-similar form already suggested by Mullins:

$$y(x,t) = \frac{m}{2}(Bt)^{1/4} Z(x/(Bt)^{1/4}), \tag{5}$$

where

$$Z^{(4)}(u) - \frac{1}{4}uZ'(u) + \frac{1}{4}Z(u) = 0, \tag{6}$$

whose general solution is

$$Z(u) = Z(0)G_0(u^4) + Z'(0)u + \frac{1}{2}Z''(0)u^2 G_2(u^4) + \frac{1}{6}Z'''(0)u^3 G_3(u^4), \tag{7}$$

where G_0, G_2, G_3 are hypergeometric functions. Condition (4) implies

$$\begin{aligned} 2\Gamma(5/4)Z(0) + \sqrt{2}Z'(0) - \sqrt{2\pi}Z'''(0) &= 0, \\ \sqrt{2}Z'(0) + 2\Gamma(3/4)Z''(0) + \sqrt{2\pi}Z'''(0) &= 0, \end{aligned} \tag{8}$$

where $\Gamma(\cdot)$ is the Gamma function.

Two parameter family of solutions to Mullins' linear model

From (5), (7), (8), we see that fixing any two of the initial conditions $\{Z(0), Z'(0), Z''(0), Z'''(0)\}$ yields a unique solution to (2) satisfying (4).

Thus (5), (7), (8) give a two parameter family of solutions to (2), (4).

While this may be known, we were uncertain where to find it in the literature. Mullins' solution as prescribed in his 1957 paper can be obtained from the description above by setting $Z'(0) = 1$, $Z'''(0) = 0$.

Are any previously unknown solution provides by this description?

At least the above description yields the following: Suppose one sets

$$Z(1) = 0, \quad Z'(1) = 1. \tag{9}$$

Then (9), (8) yields solutions which decay at ∞ and satisfy

$$y((Bt)^{1/4}, t) = 0, \quad t > 0,$$

thus explicitly describing *a decaying surface diffusion tail*.

Arc-length self-similar solutions

Together with V. Derkach (2018), we found it useful to consider (1), the 1D nonlinear surface diffusion equation, in an arc-length description

$$x = x(s,t), \quad y = y(s,t), \quad x_s^2 + y_s^2 = 1,$$

and to seek self-similar solution in terms (s,t), namely as

$$x(s,t) = (Bt)^{1/4} X(\xi), \quad y(s,t) = (Bt)^{1/4} Y(\xi), \quad \xi := s/(Bt)^{1/4},$$

see Rabkin, Klinger, Izyumora, Semenov (2000), which yields:

$$\begin{aligned} &(YX' - XY') = -4K'', \quad K = -Y'X'' + X'Y'', \quad \xi \in R^+, \\ &(X')^2 + (Y')^2 = 1, \quad \xi \in R^+, \\ &X(0) = 0, \quad Y'(0) = m/2, \quad K'(0) = 0, \quad (m = \gamma_{gb}/\gamma_s), \\ &\lim_{\xi\to\infty} Y(\xi) = \lim_{\xi\to} K'(\xi) = 0, \quad \lim_{\xi\to\infty} = 1. \end{aligned} \tag{10}$$

Mullins (1957) knew a problem for self-similar solutions to (1) could be formulated, Robinson (1971) undertook calculations, and Asai & Giga (2014) got partial results; however, their existence has not been proven. It seems the formulation in (10) is promising in this direction.

Arc-length self-similar solution calculations

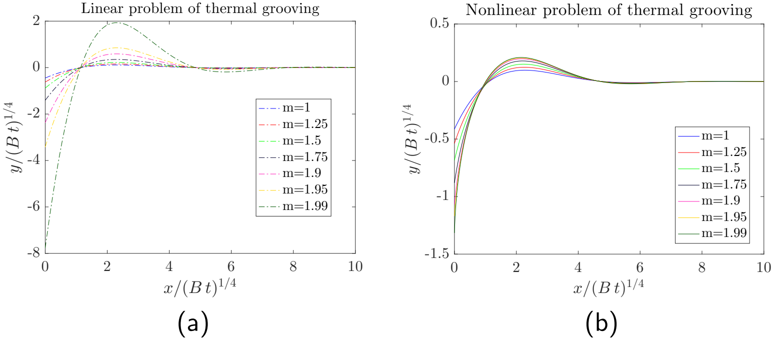

Figure 3: Solution of the linear and nonlinear BVP.

Arc-length self-similar solution calculations

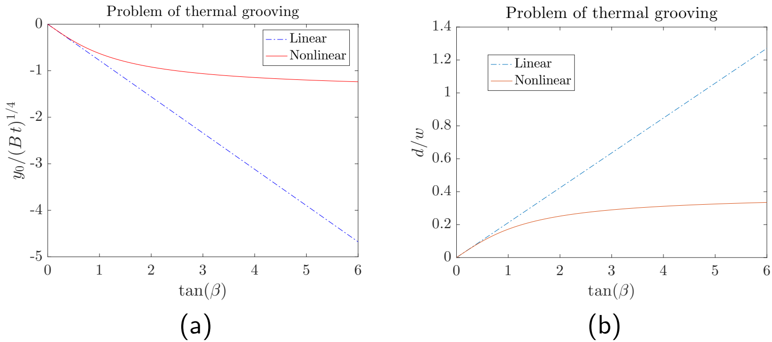

Figure 4: (a) The normalized value of y at the origin, $y_0/(Bt)^{1/4}$. (b) The ratio of the groove depth to the groove width, d/w. Here $\tan\beta = m(4-m^2)^{-1/2}$.

Steady states: I

Thin polycrystalline steady states:

spherically capped hexagonal arrays

work with V. Derkach, J. McCuan, & A. Vilenkin (2017)

Hexagonal tilings

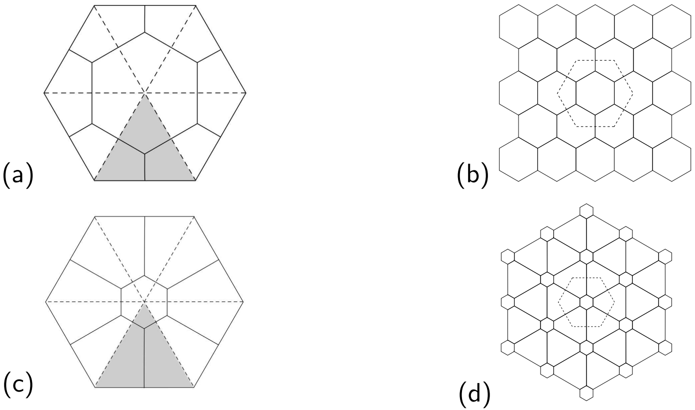

Figure 5: The triangular systems contained in the grey equilateral triangles, can be extended by mirror symmetry to yield a hexagonal tiling of R^2, see Derkach, N-C., Vilenkin & Rabkin (2014).

Truncated square and truncated hexagonal tilings

(a) (b)
(c) (d)

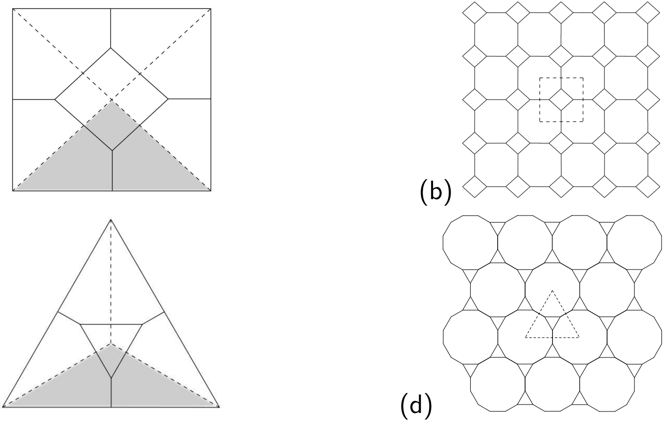

Figure 6: Reflection of the triangular systems in the grey triangles, with angles $\pi/4$, $\pi/2$, $\pi/4$ in (a),(b), and with angles $\pi/6$, $2/3\,\pi$, $\pi/6$ in (c),(d), yields truncated square tilings and truncated hexagonal tilings, respectively, of R^2.

Geometric Constructs

- Grain boundaries.
- Exterior surfaces.
- Triple junctions:
  - Thermal grooves.
  - Groove roots.
  - Interior triple junctions.
- Quadruple junctions.
- Corner points.
- The mid-plane.
- Bounding planes.

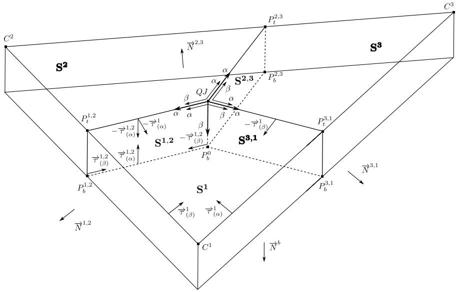

Figure 7: A typical 3 grain triangular system.

Problem Formulation Assumptions

- **Grain boundaries** evolve by (isotropic) **mean curvature motion**:

$$V_n = \mathscr{A}\, H.$$

- **Exterior surfaces** evolve by (isotropic) **surface diffusion**:

$$V_n = -\mathscr{B}\, \triangle_s H.$$

- **Conditions along thermal grooves:**.
  - Persistence.
  - Balance of mechanical forces.
  - Continuity of the chemical potential.
  - Balance of mass flux.
- **Similar conditions** along interior triple junction and at corners.
- **Symmetry** with respect to the bounding planes and the mid-plane.

Neglected: elasticity, anisotropy, evaporation/condensation, defects, . . .

Equations of Evolution

Motion by mean curvature

$$V_n = \mathscr{A}\, H. \tag{11}$$

Motion by surface diffusion

$$V_n = -\mathscr{B}\, \triangle_s H. \tag{12}$$

- V_n - normal velocity of evolving surface.
- H - mean curvature of evolving surface.
- $\triangle_s$ - the Laplace - Beltrami operator (the surface Laplacian).
- $\mathscr{A}$ - reduced mobility - the grain boundary kinetic coefficient.
- $\mathscr{B}$ - the surface diffusion "Mullins" coefficient.

1. Conditions along Thermal Grooves

X^1, X^2: exterior surfaces, X^3: grain boundary; X^1, X^2, X^3 couple along thermal groove.

Balance of mechanical forces

Young's law (isotropic Herring's law):

$$\sigma_s \overrightarrow{\tau}^1 + \sigma_s \overrightarrow{\tau}^2 + \sigma_{gb} \overrightarrow{\tau}^3 = 0. \quad (13)$$

- σ_s, σ_{gb}: exterior surface and grain boundary free energies.
- $\overrightarrow{\tau}^i$ $i = 1, 2, 3$: unit tangent vectors along thermal groove.

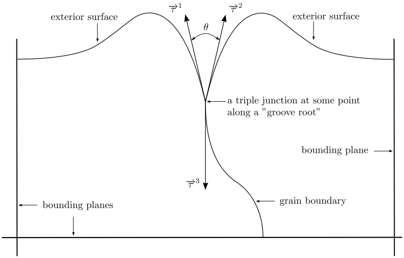

Figure 8: Groove cross-section.

- θ: the dihedral angle,

$$\theta = \pi - 2\,\arcsin\left(\frac{m}{2}\right), \quad (14)$$

$$m = \sigma_{gb}/\sigma_s,\ m \in [0, 2]. \quad (15)$$

Boundary Conditions at the Quadruple Junction

Assumptions:

- Limiting regularity at the quadruple junction: in a limiting neighborhood of the quadruple junction, triple junction lines become straight.
- Young's law holds up to the quadruple junction, on all triple junction lines.

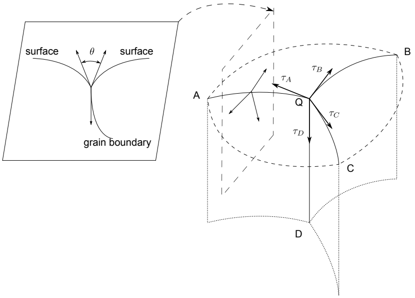

Figure 9: Sketch of a quadruple junction.

A Tetrahedron Construction and Quadruple Junction Wetting

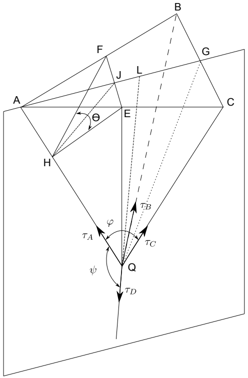

Figure 10: A tetrahedral construction at quadruple junctions, based on the tangent vectors τ_A, τ_B, τ_C.

From trigonometry, φ, ψ satisfy

$$\cos(\varphi) = -\frac{2-m^2}{4-m^2}, \qquad (16)$$

$$\cos(\psi) = -\frac{1}{\sqrt{3}}\frac{m}{\sqrt{4-m^2}}, \qquad (17)$$

$$0 \le \varphi \le \frac{2\pi}{3}, \quad \frac{\pi}{2} \le \psi \le \pi, \qquad (18)$$

require that $m \in [0, \sqrt{3}] \subset [0, 2]$.

Breakdown of the construction:

$m = \sqrt{3}$ **as a quadruple junction wetting condition, Derkach, 2010.**

See also Smith 1948, Taylor 1976, Straumal et.al. 2007.

Hexagonal Tilings with Spherical Caps

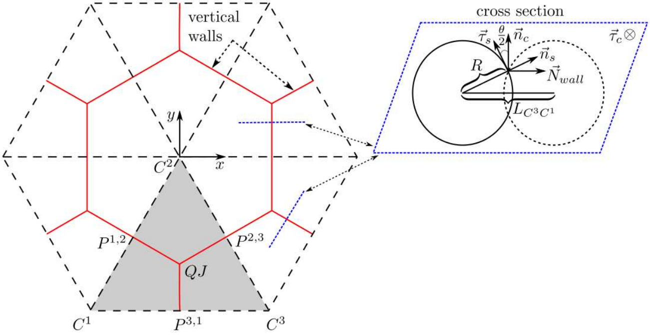

Figure 11: The triangular system within the grey equilateral triangle extends by mirror symmetry to yield a hexagonal tiling. The exterior surfaces above the hexagons are spherical caps of radius R, intersected by grain boundaries which are planar and normally intersect the xy plane. All dihedral angles equal θ. See also Srolovitz & Safran (1986).

A Tetrahedron Construction and Quadruple Junction Wetting

The spherical caps intersect the flat vertical grain boundaries along circular sections, with maximal height relative to the the spheres' centers $z_{\max} = (L_{C^3C^1}\sqrt{4-m^2})/(2m)$, and with minimal height $z_{\min} = (L_{C^3C^1}\sqrt{3-m^2})/(\sqrt{3}m)$, attained at the quadruple junctions. The construction requires $0 < m < \sqrt{3}$, implying $m \geq \sqrt{3}$ as a quadruple junction wetting criterion. The **nonexistence result** below implies this restriction is sharp.

Theorem. Given a domain Ω with a corner with interior angle α. If $\alpha + \theta < \pi$ there exist no constant mean curvature surfaces defined over Ω which are bounded from below and meet $\partial\Omega$ with contact angle $\theta_c = \frac{1}{2}(\pi - \theta)$. **Proof.** See Finn [Corollary 5.5] and definitions there.

For the equilateral triangular system, $\alpha = \frac{2\pi}{3}$, $\theta = 2\cos^{-1}(m/2)$, and the restriction $\alpha + \theta < \pi$ implies non-existence of solutions bounded from below if $m > \sqrt{3}$. If non-boundedness occurs, it occurs at the vertex of the interior corner. So for spherical capped hexagons, any such steady states necessarily penetrate the film at the quadruple junction.

A Tetrahedron Construction and Quadruple Junction Wetting, 2.

For thin films, the film thickness required to guarantee film stability is a technologically critical issue. This leads us to consider volume restrictions for the realization of these configurations. The volume of the spherical cap over the hexagon and above height $z_{\min}$ is given by

$$V^{cap} = L^3_{C^3C^1}\left[\mathcal{F}(m) - \frac{\sqrt{3-m^2}}{2\,m}\right], \qquad \text{where}$$

$$\mathcal{F}(m) = \frac{3}{2}\int_0^1 \left[\frac{\xi\sqrt{3-m^2\,\xi^2}}{3\,m} + \frac{4-m^2\,\xi^2}{2\,m^2}\,\text{arcsin}\left(\frac{m\,\xi}{\sqrt{3}\,\sqrt{4-m^2\,\xi^2}}\right)\right]d\xi.$$

Letting L_z^* denote the height of a flat configuration with equivalent volume, namely the height L_z^* such that $V^{cap} = \frac{\sqrt{3}}{2}L_z^* L^2_{C^3C^1}$, we obtain that realization of the capped hexagon configuration requires that

$$L_z \geq L_z^* = \frac{2}{\sqrt{3}}\left[\mathcal{F}(m) - \frac{\sqrt{3-m^2}}{2\,m}\right] L_{C^3C^1}.$$

Note in particular that if $m = 0.3$, then $L_z^* \approx 0.02946 L_{C^3C^1}$.

Are spherically capped hexagons energetically preferable, when realizable?

For the capped hexagons

$$E_w^{cap} = L_{C^3C^1}^2 \mathcal{G}(m) + \sqrt{3}\, m L_z L_{C^3C^1}, \quad \mathcal{G}(m) \text{ known,} \tag{19}$$

and for the equivalent volume flat configuration with flat grain boundaries

$$E_w^{initial} = \frac{\sqrt{3}}{2} L_{C^3C^1}^2 + \sqrt{3}\, m L_z L_{C^3C^1}. \tag{20}$$

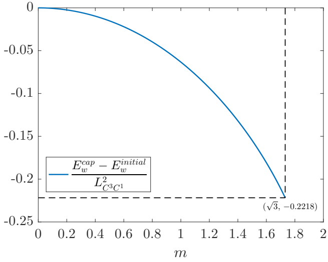

Figure 12: We see clearly that $E_w^{cap} \leq E_w^{initial}$.

A Tetrahedron Construction and Quadruple Junction Wetting, 4.

Above, energies were compared for configurations with the same volume, and the length, $L_{C^3C^1}$, of side of the bounding triangle was fixed.

From the geometry, $L_{hexagon} = \frac{1}{\sqrt{3}} L_{triangle} = \frac{1}{\sqrt{3}} L_{C^3C^1}$.

Let us now compare the energies for spherically capped hexagon configurations with the same volume, allowing the length of the triangle (hexagon) side to vary. Fixed V implies that the height of the equivalent volume flat triangular system satisfies $L_z = \frac{2}{\sqrt{3}} V L_{C^3C^1}^{-2}$. So by (19)

$$E_w^{cap} = L_{C^3C^1}^2 \mathcal{G}(m) + \frac{2mV}{L_{C^3C^1}}, \tag{21}$$

which attains a minimum at

$$L_{C^3C^1}^{\min} = \left[\frac{mV}{\mathcal{G}(m)} \right]^{\frac{1}{3}}. \tag{22}$$

We conjecture that (22) is indicative of an energetically preferred length scale for grains with prescribed volume in a bamboo structured system.

A Tetrahedron Construction and Quadruple Junction Wetting, 5.

Should coarsening be expected to ensue in the spherically capped system? It follows from (19) that the weighted energy per unit area of the capped hexagon system is given by

$$\frac{2}{\sqrt{3}}\,\frac{E_w^{cap}}{L^2_{C^3C^1}} = \frac{2}{\sqrt{3}}\,\mathcal{G}(m) + \frac{2mL_z}{L_{C^3C^1}}. \tag{23}$$

Since (23) decreases as $L_{C^3C^1}$ increases, there is an energetic preference for coarsening. However coarsening may be hindered by dynamic considerations such as local energy barriers.

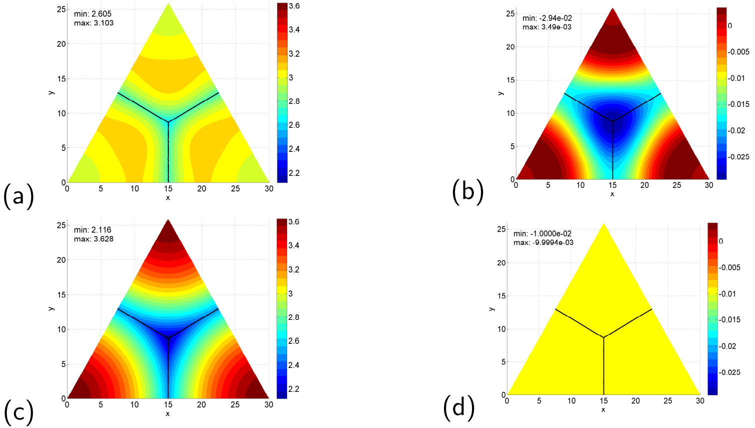

Figure 13: Here $\phi_{C^1} = \phi_{C^2} = \phi_{C^3} = 1/3$, $L_{C^1C^2} = 30$, $L_z = 3$ and $m = 0.3$. The exterior surfaces heights, (a) for $t = 50$ and (c) for $t = 6300$. The exterior surfaces mean curvatures, (b) for $t = 50$ and (d) for $t = 6300$. The grains remain symmetric and the mean curvatures converges $\approx \frac{m}{L_{C^1C^2}} = 10^{-2}$, as in the steady state discussed.

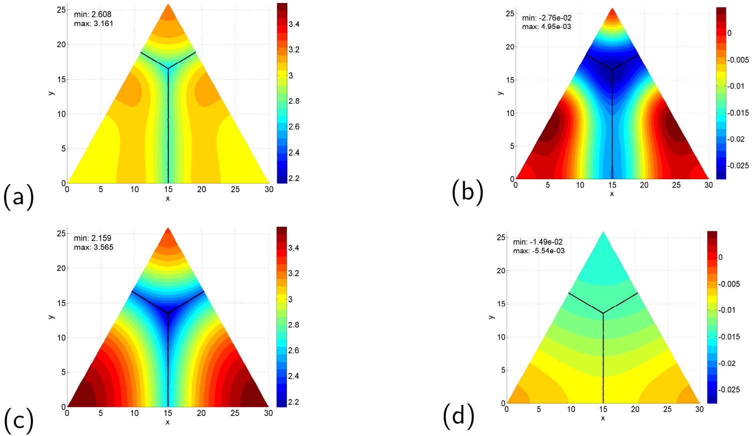

Figure 14: Here $\phi_{C^1} = \phi_{C^3} = 0.45$, $\phi_{C^2} = 0.1$, $L_z = 3$ and $m = 0.3$. The exterior surface heights, (a) for $t = 50$ and (c) for $t = 2310$. The exterior surface mean curvatures, (b) for $t = 50$ and (d) for $t = 2310$. The smaller grain grows, and the system seems to approach the earlier steady state.

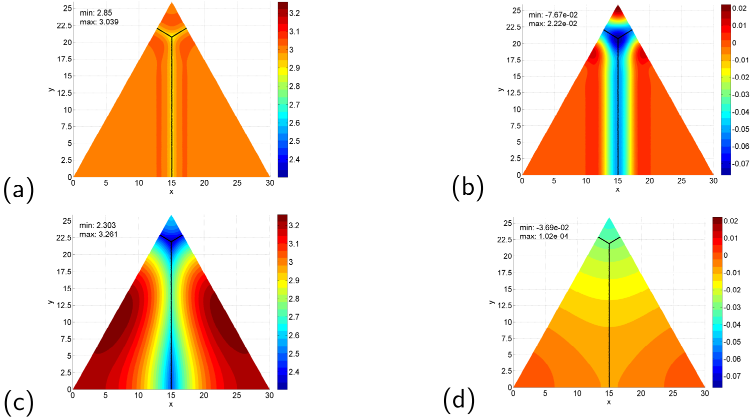

Figure 15: Here $\phi_{C^1} = \phi_{C^3} = 0.485$, $\phi_{C^2} = 0.03$, $L_z = 3$ and $m = 0.3$. The exterior surface heights, (a) for $t = 1$ and (c) for $t = 703$. The exterior surface mean curvatures, (b) for $t = 1$ and (d) for $t = 703$. We observe shrinkage and sinking of the smaller grain. Apparently if initially one grain is much smaller than the others, the steady state with three fold symmetry is not approach.

Steady states: II

Axi-symmetric 2 grain systems:

within a finite radius cylinder

joint work with V. Derkach & J. McCuan

Axi-symmetric equilibria:

We consider rotationally symmetric equilibrium configurations consisting of two grains. The cross-section we have in mind is indicated in Fig. 16.

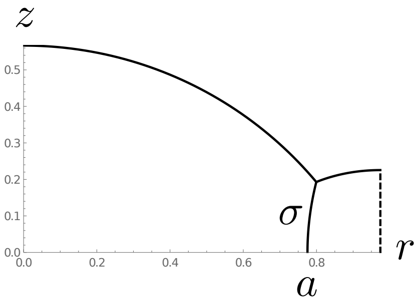

Figure 16: Cross-section of an axi-symmetric equilibrium. Here a is the width of the catenoid neck and σ is the arclength of the catenoid from its neck to the triple-junction. The cylinder radius has been normalized to unity.

Axi-symmetric equilibria: cont.

We find for fixed $m \in (0,2)$, or equivalently for fixed $\beta = \arctan(\frac{-m}{\sqrt{4-m^2}})$, that there is a two parameter family of equilibria for a finite cylinder of radius 1 which are composed of

1) a portion of a **sphere** with radius R_0 which meets the axis at a right angle,

2) a portion of a **plane** which is orthogonal to the axis or a **catenoid**:

$$r = \alpha \cosh(z/a),$$

both of which have zero mean curvature,

3) a portion of a **nodoid**, with mean curvature $-1/R_0$, which intersects the bounding cylinder at a right angle. The inclination angle ψ along the nodary median satisfies

$$\sin \psi = -\frac{1}{R_0}\left(r - \frac{1}{r}\right).$$

Axi-symmetric equilibria: parametrization

The various conditions imply the following constraint:

$$\frac{a\cos\beta+\sigma\sin\beta}{\sigma\sin\beta-a\cos\beta}=1-\frac{1}{\sigma^2+a^2}, \tag{24}$$

which may also be written as:

$$a^3+\left(\sigma^2-\frac{1}{2}\right)a+\frac{\sigma\tan\beta}{2}=0.$$

From (24), we may conclude:

Theorem. For fixed $\beta\in(\pi/2,\pi)$, there is a smooth function $a=a(\sigma)$ defined for $0\le\sigma\le-\cos\beta$ by (24), with $a(0)=\frac{1}{\sqrt{2}}$, $a(-\cos\beta)=\sin\beta$. The graphs $\Gamma_\beta=\{(a(\sigma),\sigma):0<a<-\cos\beta\}$ for $\pi/2<\beta<\pi$ foliate $\mathcal{R}=\{(a,\sigma):1/2<a^2+\sigma^2<1,\ a,\sigma>0\}$, see Fig. 17.

Axi-symmetric equilibria: parameter domain

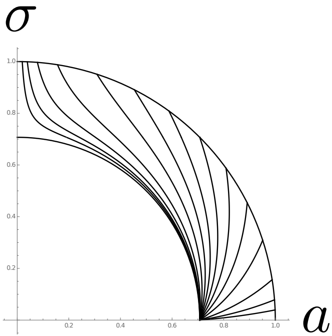

Figure 17: Parameter domain for equilibrium configurations for fixed β.

Acknowledgements

Thank you for your interest!